Med Biol Eng Comput (2012) 50:493–502
DOI 10.1007/s11517-012-0891-y

ORIGINAL ARTICLE

Haemodynamic forces on in vitro thrombi: a numerical analysis

Christopher J. Butler · Kris Ryan · Gregory J. Sheard

Received: 9 August 2011 / Accepted: 1 March 2012 / Published online: 16 March 2012

Abstract The flow of blood past an axisymmetric thrombus analogue, within an in vitro geometry, is computed via solution of the discrete three-dimensional (3D) Navier–Stokes equations. Particle tracking is used to model the behaviour of thrombocytes (platelets) moving throughout the domain and to investigate behaviour with respect to the platelets. The system is explored using shear rate to quantify the effects an idealised thrombus has with respect to an undisturbed in vitro geometry over 'Poiseuille flow' shear rate conditions applicable to in vivo and in vitro experiments (1,200–10,000 s^{-1}). Local shear rate variations show peaks in shear rate greater than double that of Poiseuille flow conditions. These local shear rate variations are observed to be non-linear, despite the low Reynolds number (5.2–43.4) within the system. Topological transitions of shear rate are observed, limiting the height of peak shear rate within the system, suggesting a thrombus growth limiting behaviour. Temporal gradients of shear rate, measured with respect to individual platelets, were calculated. Multiple regions of peak shear rate gradient were observed throughout the flow, suggesting that platelet–platelet interaction may not be limited to regions near to the surface of the thrombus.

Keywords Platelet adhesion · Shear rate · Thrombus · Micro-channel

C. J. Butler · K. Ryan (✉) · G. J. Sheard
Fluids Laboratory for Aeronautical and Industrial Research (FLAIR), Department of Mechanical and Aerospace Engineering, Monash University, Melbourne, VIC 3800, Australia
e-mail: kris.ryan@monash.edu

1 Introduction

The development of thrombi presents a significant clinical risk of myocardial infarction, cerebral and pulmonary embolism, and other diseases (for reviews see [12, 25] among others). However, understanding the effect of physical forces on thrombi development remains poorly understood [5]. Under arterial conditions, the structure of a thrombus is dominated by platelets adhered together within a fibrin matrix. Biochemical processes governing the formation of the platelet–fibrin structure is well understood [2, 8, 9]. However, the process of platelet adhesion is dependent on the physical forces exerted by blood on an individual platelet. Exactly how platelet adhesion is affected by these forces is unclear.

Early studies [4] showed a correlation between the haemostatic action of platelets and the shear stresses exerted by the working fluid on the platelets. In these studies shear stresses were measured in terms of shear rate (γ $(1/s)$). These early discoveries were only delineated between pathological and normal functionality. Recently, a clearer picture of the effect of mechanotransduction on platelet hemostasis has been developed for the full range of biologically relevant shear rates.

Platelet adhesion under shear is typically investigated in high aspect ratio rectangular micro-channels. This geometry is chosen as steady flow within the channel, away from any entrance or exit effects, is well described by Poiseuille flow. Under Poisuielle flow conditions the wall share rate (γ_{Pw}) may be considered constant for a given flow rate. Consequently, many previous studies employed the Poiseuille flow wall shear rate (γ_{Pw}) to characterise the shear rate environment (details of different techniques for calculating γ are described in Sect. 2.1).

Many previous studies (e.g. [7, 13, 15, 19, 20]) treated the shear rate within the micro-channels as a constant. For

an empty channel (without thrombi), with the high aspect ratio channels (10:1 or greater) employed, this is an adequate characterisation of the surface shear environment. However, recent research has revealed that platelet adhesion is dependent on a spatial microgradients gradient of γ [16], and temporal gradients of γ_{Pw} [10]. This behaviour was observed both in vivo and in vitro. Additionally, the platelet aggregation was shown to be driven by von Willebrand Factor (vWF)-based bonding in the absence of platelet activation [15, 16] and is therefore driven by localised mechanotransduction.

The introduction of this new paradigm poses a problem with respect to quantifying the shearing stresses that blood exerts on its constituent platelets. Shear rate, even within simplified, steady-state flow, and nearly two-dimensional environments is no longer independent of position (with respect to a given thrombus). Rather, the flow past a simple object such as a thrombus is three-dimensional with localised variations in γ. This is clearly demonstrated in both [16, 24], via a limited number of computational fluid dynamics analyses. In addition, Tolouei et al. [24] measured a linear relationship between mature thrombus height and γ_{Pw}. We hypothesise that the imposition of the thrombus on the channel imposes results in a non-linear change in peak shear rate, as used to quantify shear variations in [16], with respect to both γ_{Pw} and the size of the thrombus. Additionally, we hypothesise that in addition to the changes in peak shear rate, the topology of shear rate surrounding thrombus. Nesbitt et al. [16] highlighted the importance of gradients of shear rate but did not explore temporal gradients with respect to shear rate. Here, complex variations in shear rate (temporal) gradient are anticipated with respect to position and thrombus size.

2 Methods

In designing the model and parameter space considered within this paper, there were two key aims: closely matching the environments observed experimentally, and creating a simple model such that the parameter space can be established without prohibitive computational cost. Kulkarni et al. [14] describe the methodology, and geometry, used commonly in in vitro experiments. Our study has created a numerical model of the 'micro-channels' described in [14]. Consequently, the model channel has a width to height ratio of 10:1. The channel is presumed to be long with respect to cross-section such that any entrance or exit effects may be safely ignored. The Reynolds number range was selected in order to match the conditions in the channel specified by Kulkarni et al. [14] as 'intermediate'. This matches the domain, and the flow conditions, used by Dopheide et al. [7], Nesbitt et al. [16], Tolouei et al. [24] and others. This gives us a system where the Reynolds number (Re) is proportional to γ_{Pw}, and is written

$$Re = 4.34 \times 10^{-3}\gamma_{Pw}. \quad (1)$$

The Reynolds number (Re) is defined as

$$Re = \frac{\bar{U}H}{v}, \quad (2)$$

where $\bar{U}$ is the mean flow velocity, H the height of the channel and v the kinematic viscosity.

Blood is strictly categorised as a non-Newtonian fluid. However, under steady-state conditions and high shear rates (such as considered here), blood behaves as a Newtonian fluid [18]. This is inherent in the Poiseuille flow assumption previously employed. Therefore, this study considers the flow of blood as a incompressible, unsteady, and Newtonian fluid within the channel. This approximation yields the Navier–Stokes equations as

$$\frac{\partial \mathbf{u}}{\partial t} + \mathbf{u} \cdot \nabla \mathbf{u} = -\nabla P + v\nabla^2 \mathbf{u}, \quad (3)$$

$$\nabla \cdot \mathbf{u} = 0, \quad (4)$$

where $\mathbf{u}$ is the velocity vector, and $P = p/\rho$ is the kinematic pressure field (pressure p normalised by fluid density ρ).

Into this channel we introduce a thrombus analogue, represented by a partially protruded sphere, located at the centreline of the channel. Figure 1 shows an isometric representation of the sphere. The sphere was placed along the channel centerline to minimise any effects from the side walls of the channel.

A cylindrical, and thus axisymmetric, numerical domain, centred on the thrombus, is extracted from the channel. This is represented by the translucent grey cylinder in Fig. 1. At the numerical domain's maximum extent its boundary is located such that it coincides with the side walls of the modelled channel.

The axisymmetric geometry allows the numerical domain to be defined within a meridional semi-plane shown in Fig. 1b. The geometry is defined as follows: given the 10:1 channel aspect ratio, the mesh radius, W, to height, H, is $W/H = 5$. The model thrombus itself is defined on the axis such that the thrombus maintains geometric similarity throughout these studies. That is, the ratio of thrombus height, H_T to thrombus radius, r, is kept constant

$$\frac{H_T}{r} = 0.5. \quad (5)$$

This value was chosen in consultation with the authors of [24] as a simplified thrombus representation. The thrombus height is non-dimensionalised as a fraction of the channel height

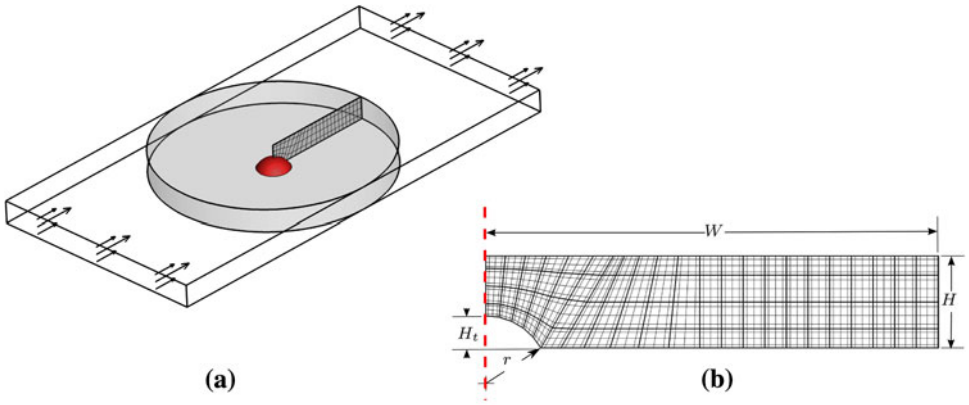

Fig. 1 Representation of the numerical domain within the microchannel. **a** An isometric view of the channel. A section of the channel is outlined with *dashed lines*. The flow direction is indicated with the *black arrows*. *Shaded cylindrical region* The numerical domain containing the thrombus (*shaded red*). Note that the numerical domain occupies the full width of the channel. The mesh within the computational domain is shown in detail in **b**. **b** A representative (r–z) plane. Spectral-element boundaries are denoted by *bold lines*. *Thin grey lines* Nodal evaluation points within elements. *Dashed red line* The axis of rotation (colour figure online)

$$h_t = \frac{H_T}{H}. \tag{6}$$

For each γ_{Pw}, 21 different thrombus heights are considered over $0.02 \leq h_t \leq 0.8$.

The momentum equation (Eq. 3) is numerically integrated in weak form using a third order dual operator-splitting scheme [11]. The integration scheme, first implemented in [23], is solved in primitive variable form using a spectral-element technique. This study computes the flow in a cylindrical coordinate system [21]. As the cylindrical domain chosen for this problem is spatially periodic in the azimuthal direction, the azimuthal direction consequently is discretised using a Fourier expansion allowing p-type refinement. The meridional (z–r) plane is discretised by a mesh of quadrilateral spectral-elements employing tensor–product Gauss–Lobatto–Legendre (GLL) interpolants, a example of this discretisation is shown in Fig. 1b. This spectral-element/Fourier solver is an implementation of the method described by Blackburn and Sherwin [3]. Grid independence studies were performed both with respect to the number of Fourier modes azimuthally (N_m) and the order of the GLL polynomials N_p in the z–r plane. The resolution study resulted in selecting $N_p = 10$ and $N_m = 41$ in a region where exponential convergence was observed. Error measured with respect to the highest resolution case was less than 0.001 %.

The top and bottom boundaries of the mesh are located at the channel walls. These boundaries and the thrombus surface have a no-slip boundary conditions applied. Curvilinear elements are used to accurately resolve the curvature of the model thrombus. The axis of rotation has boundary conditions as stipulated in [3] which allows flow to cross the axis. The (radially) outer boundary is more complex. Given that this domain is contained within a finite width channel, around this cylindrical boundary the analytical solution for fully developed flow through a rectangular cross-sectioned channel was imposed [17, p. 112].

2.1 Calculating local shear rate

Historically, shear rate, rather than shear stress, has been used to measure the influence of shearing stresses on thrombotic geometries. Most previous investigations have considered shear rate only under Poiseuille flow—specifically, the maximum in shear rate that occurs at the walls in Poiseuille flow (Eq. 9). However, Nesbitt et al. [16] and Tolouei et al. [24] revealed flaws in this methodology, identifying that local variations in shear are significant within the in vitro geometry. Formally, shear rate at a given location in three dimensions may be defined as

$$\gamma_T = \nabla \mathbf{u} + (\nabla \mathbf{u})^{\mathsf{T}}, \tag{7}$$

where γ_T is the shear rate defined as a tensor. However, given an isotropic (Newtonian) fluid, the shear rate is reduced to a scalar,

$$\gamma = \sqrt{0.5 \times \gamma_T : \gamma_T}, \tag{8}$$

where the (:) operator denotes a matrix inner product. Throughout this paper this is the form of scalar shear rate used. Additionally, we define γ_{Pw}, the Poisuille flow wall shear rate as

$$\gamma_{Pw} = \frac{6\bar{U}}{H}. \tag{9}$$

Hereafter, shear rates are expressed normalised by γ_{Pw}, represented by $\chi = \gamma/\gamma_{Pw}$.

2.2 Platelet transport

Solution of the discrete Navier–Stokes equations provides an understanding of the flow; however, it does not directly show the history of stresses experienced by platelets. In order to model the experiences of platelets, a particle transport method is employed. This allows the simulation of the flow of platelet analogues, which are particles, throughout the domain. From this, predictions can be made on the physical stimuli, including shear rate, that platelets experience.

The particles, as platelet analogues, are introduced as massless, infinitesimal spheres. Platelet trajectories are calculated using a method proposed by Coppola et al. [6], which makes full use of the high-order velocity field information to achieve accurate trajectories. This implementation has recently been validated in [22] for the three-dimensional formulation and maintains the higher-order resolution of the spatial discretisation. This model is valid for platelets under conditions where blood may be modelled as a continuum.

Given the size of the platelets are small with respect to the flow, the difference in shear rate felt across the surface is negligible. Consequently, platelets cannot directly feel a gradient in shear. Rather they experience a temporal gradient in shear rate

$$\psi = \frac{\mathrm{D}\chi}{\mathrm{D}t^*}, \tag{10}$$

where t^* is time (t) normalised by a characteristic time (T)

$$T = \frac{H}{\bar{U}}. \tag{11}$$

To investigate the behaviour of the temporal shear rate gradient, ψ, two methods were used: taking a snapshot in time mapping the platelet information to space, in particular ψ, across space; and evolving platelets throughout the domain to provide a history of ψ as the platelets flow past the thrombus.

The first 'Platelet mapping' process is achieved by approximating ψ for platelets using a second order Taylor series approximation for the time derivative on platelets seeded throughout the domain at a high density. The ψ data located at the platelets are re-interpolated onto the Eulerian grid for visualisation, using a radial basis function interpolation scheme over a number of sub-domains.

In order to track the process of platelets throughout the domain, a two-dimensional grid of platelets is introduced at a plane perpendicular to the flow, upstream of the thrombus. The platelets are evolved through time until they exit the domain. Checkpoints of the data are regularly taken during this evolution. For each particle, an Akima cubic spline [1] is fitted to the shear rate data throughout time. This allows the analysis of particle data such that the behaviour of a platelet can be considered with respect to its location in undisturbed flow.

3 Results

3.1 Shear rate maximum

The shear rate was determined at each nodal evaluation point, for all Fourier planes, within the solution. The maximum shear rate, $\hat{\chi}$, was taken as the peak value across the nodal points of the solution. A map of $\hat{\chi}$ was obtained across all of the simulated cases is shown in Fig. 2. In every case considered within this study, $\hat{\chi}$ is found to be located on the surface of the model thrombus.

For a given γ_{Pw} the shear rate peaks at the point where the thrombus size is at the minimum simulated ($h_\mathrm{t} = 0.02$). As the thrombus size increases towards $h_\mathrm{t} \simeq 0.5$, $\hat{\chi}$ decreases. The most significant factor generating the shear rate decrease is the corresponding decrease in curvature of the thrombus. As the thrombus analogue maintains geometric similarity the curvature is inversely proportional to h_t. The surface curvature induces rotation in the fluid causing increases in shear rate. Thus, the high curvatures at small thrombus sizes result in significantly higher shear rates. However, the decreasing thrombus size also results in a corresponding decrease in the size of high shear regions.

At $h_\mathrm{t} \simeq 0.5$, a local minimum of $\hat{\chi}$ is observed for each γ_{Pw}. As the thrombus continues to increase in size past $h_\mathrm{t} \simeq 0.5$ so does $\hat{\chi}$. The increase in $\hat{\chi}$ is attributed to the increasing percentage of the channel blocked by the thrombus (up to 15 % of the channel based on cross-sectional area). The higher blockage accelerates the flow around the thrombus. Consequently larger velocity gradients and shear rates are observed. The blockage is proportional to h_t^2, and occurs throughout the full range of h_t, however, at small h_t, the increase in $\hat{\chi}$ due to blockage is small with respect to the effects of curvature.

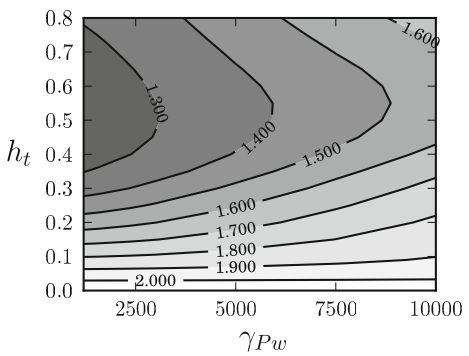

Fig. 2 Peak shear rate, $\hat{\chi}$, plotted against h_t and γ_{Pw}. *Darker* and *lighter shading* represent smaller and larger values of $\hat{\chi}$, respectively

At all h_t an increase in non-dimensionalised shear (χ) is observed with increasing γ_{Pw}. Given that shear rate is normalised by γ_{Pw}, the increase is non-linear with respect to γ_{Pw}, and therefore Reynolds number. This clearly shows that the bulk approximation for shear rate (Eq. 9) is insufficient to characterise the system at biologically relevant Reynolds numbers. This is in contrast to Poiseuille flow, which, due to the simple geometry, becomes Reynolds number independent. Therefore, overall behaviour of the maximum shear rate is dependent on both geometry and the bulk flow properties (γ_{Pw}).

The dependence of the localised shear rate behaviour, while intuitive from a fluid dynamics perspective, is important to the biology of the system. In particular, it limits the ability to generalise laboratory experimental results across a large range of shear rates.

3.2 Location and profile of shear rate maxima

Section 3.1 showed gradual yet significant changes in the magnitude of the peak χ with respect to both h_t and γ_{Pw}. Consequently a similar behaviour is expected with respect to the profile of shear rate contours and location of the shear rate maximum. Figures 3 and 4 examine representative behaviour of the system.

Figure 3 shows contours of the shear rate on the surface surrounding the thrombus, and the surface of the thrombus, as the thrombus size increases. This is consistent with self-similar growth of a thrombus within the in vitro channel considered by [24]. The figure shows results at $\gamma_{Pw} = 3{,}000$, which can be considered typical of our results for all γ_{Pw} considered. Contours at the surface are visualised as they show the extreme values of χ throughout the fluid volume. It should be noted that χ approaches zero at the centre of the channel cross section.

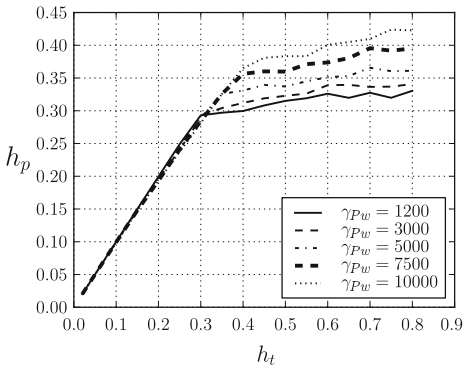

Fig. 4 Height at which the peak shear rate is found (as a fraction of channel height) plotted against normalised thrombus height, for channel γ_{Pw} as shown

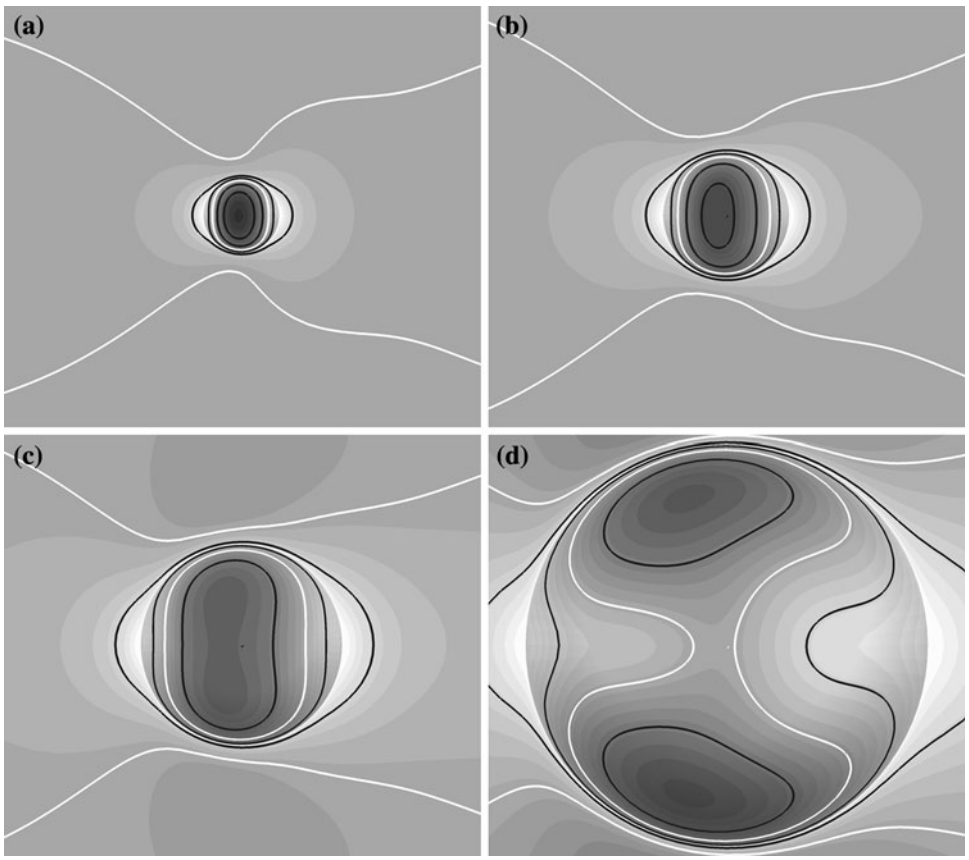

Fig. 3 Contours of normalised shear rate, χ, plotted on the lower channel wall and the surface of the thrombus. $\gamma_{Pw} = 3{,}000$ in each frame, which is representative of the behaviour for all γ_{Pw} considered in this study. The thrombi size varies such that $h_t = 0.15, 0.25, 0.4, 0.8$ for frames **a** through **d**, respectively. Flow is from left to right. Both *black* and *white contour lines* represent values of χ. The *white contours* are of the value $\chi = 1$, *black contours* occur at increments of $\Delta\chi = 0.25$ away from the level $\chi = 1$. *Darker* and *lighter shades* of *grey* represent larger and smaller values of shear rate, respectively

Figure 3a, b displays evidence of the behaviour expected from [16]. Specifically, a single peak in shear rate is found on the thrombus surface. Nesbitt et al. [16] focused on two aspects of this flow: the region of high shear rate localised at the thrombus and the low shear rate region at the thrombus trailing edge. However, these results demonstrate that an additional low shear region is observed locally in front of the thrombus. This low shear region is due to localised stagnation of the flow as it approaches the thrombus. This zone would be observable for all thrombi protruding into the flow, regardless of specific thrombus profile.

Figure 3c, d displays contrasting flow features. In the same manner as Fig. 3a, b, low shear regions are located at the leading and trailing edges of the thrombus. However, rather than a single peak of shear rate appearing on the centreline of the thrombus, there instead exist two peaks of shear rate, which are located symmetrically left and right of the centreline of the channel. Therefore, as the thrombus size increases, the central peak splits into two peaks. This process can clearly be seen in the progression through frames (b)–(d) of Fig. 3. Examination of the same heights at differing γ_{Pw} shows the shear rate peaks moving forward (data not shown).

In each simulation considered the location of the peak shear rate ($\hat{\chi}$) is determined. For all the cases considered, the location of $\hat{\chi}$ is on the thrombus surface. Therefore, the characteristics of the behaviour may be examined using h_{p}, the normalised height of peak shear rate within the channel defined as

$$h_{\mathrm{p}} = \frac{H_{\mathrm{p}}}{H}. \tag{12}$$

where H_{p} is the physical height within the channel.

The resultant plot (Fig. 4) clearly indentifies two regions which correspond to the two behaviours observed in Fig. 2. Firstly, for $h_{\mathrm{t}} \lesssim 0.3$, the height of the peak shear rate (h_{p}) is approximately equal to h_{t}. As γ_{Pw} increases so does the magnitude of the difference between h_{t} and h_{p}. At $0.3 \lesssim h_{\mathrm{t}} \lesssim 0.5$ a transition occurs. Rather than following close to $h_{\mathrm{t}} = h_{\mathrm{p}}$ for each γ_{Pw}, an abrupt transition occurs beyond which h_{p} plateaus with respect to h_{t}. This transition occurs simultaneously with the movement of the peak shear rate locations off the flow centreline, observed in Fig. 3. The transition height (the height h_{p} plateaus towards) is found to be weakly dependent on γ_{Pw}. In summary, we note that non-linear behaviour is observed throughout the system. Both the strength and location of the peak shear rate are dependent on the thrombus size, and γ_{Pw}.

3.3 Lagrangian results

Consider a platelet introduced far upstream of the thrombus at a height h_{i} from the surface. A number of platelets travelling close to the surface along the thrombus (and channel) centreplane are shown in Fig. 3. Figure 5 shows the shear rate experienced by a number of these platelets. Here the axis of flow, x, is the horizontal axis of the plot. First we examine shear rate variations close to the surface $h_{\mathrm{i}} = 0.05$; far upstream of the thrombus χ is at the value expected for Poiseuille flow condition. On approaching the thrombus, a local minimum of χ, which occurs near the thrombus leading edge, is observed. This results in a small, yet rapid, decrease in χ. This is followed by a rapid increase in χ as the platelet passes the apex of the thrombus. As the platelet passes down the lee side of the thrombus and away into the free-stream, χ rapidly decreases as the platelet approaches the trailing edge of the thrombus. This is followed by a gradual restoration to the expected Poiseuille flow χ in the free-stream. Note that the presence of the thrombus has resulted in local minima of shear rate near the thrombus, even for biologically high γ_{Pw}. Consequently the 'low–high–low' behaviour, described within [16], still exists; however, it is augmented by higher far-field conditions. Therefore, the low–high–low behaviour may be thought of as deviations away from the far-field conditions, rather than absolute values.

When we examine the other h_{i} for Fig. 5 we notice that the behaviour changes. As the introduction height decreases, so too does the free-stream χ. As the height increases the behaviour changes, the low shear rate (with respect to the free-stream) regions rapidly disappears. A transition is noted from a single shear peak ($h_{\mathrm{i}} = 0.05$) to two distinct shear peaks ($h_{\mathrm{i}} = 0.35$).

A slight asymmetry is observed throughout the figure. One consequence of this is that for all cases, the maximum recorded magnitude of ψ for a platelet (i.e. $\max\|\psi\|$) occurs when $\psi > 0$. This is attributed to the forward/backward asymmetry of the peak of χ. It is noted that despite this asymmetry, the positive and negative amplitudes of ψ are of the same order. This is expected to be true for corresponding in vitro geometries. The extrema of ψ are explored in Figs. 6 and 7.

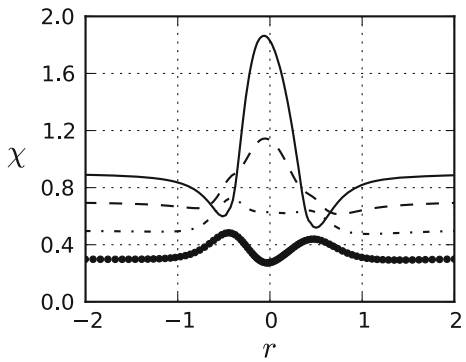

Fig. 5 Typical shear profiles for platelets travelling past the thrombus. This case shows $\gamma_{\mathrm{Pw}} = 3{,}000$, $h_{\mathrm{t}} = 0.25$. The platelets are introduced at $h_{\mathrm{i}} = 0.05, 0.15, 0.25, 0.35$, respectively, for *solid line*, *dashed line*, *dashed dotted line*, and *dotted thick line*

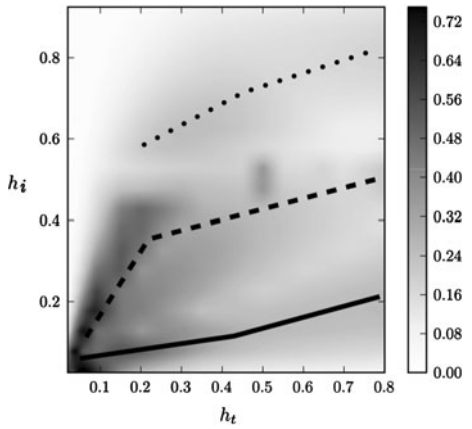

Fig. 6 Shear rate gradient maximum (Dχ/Dt*) map for $\gamma_{Pw} = 3{,}000$. The *horizontal axis* is the height of the thrombus (h_t) and the *vertical axis* the introduction height of the platelet (h_i) in the undisturbed Poiseuille flow upstream. The *greyscale contours* show *darker* and *lighter contours* as higher and lower values of shear rate maximum, respectively. *Three lines* mark the peaks within the system. They are labelled as P_1 (*solid line*), P_2 (*dashed line*) and P_3 (*dotted line*)

Figure 6 shows results calculated using the particle evolution technique, plotting data with respect to its undisturbed location. The interest in ψ stems from the results of [10], where global changes of γ_{Pw} triggered increased thrombus adhesion. For Fig. 6 the variable of interest is max$\|\psi\|$. The behaviour relative to the upstream location is plotted as within a blood vessel platelets are not uniformly distributed. Higher concentrations occur closer to the vessel walls.

The particles employed to generate Fig. 6 were introduced a distance $4H$ upstream of the thrombus. The particles were introduced in a regular grid perpendicular to the flow direction with a spacing of 0.01 H. Each of these platelet analogues is evolved past the thrombus. For each platelet analogue ψ is calculated at each timestep. From this information max$\|\psi\|$ is determined for each platelet analogue. Figure 6 plots max$\|\psi\|$ against both h_t and h_i, where h_i is the introduction height of the platelet analogues. The effects of horizontal position on the results is not explored.

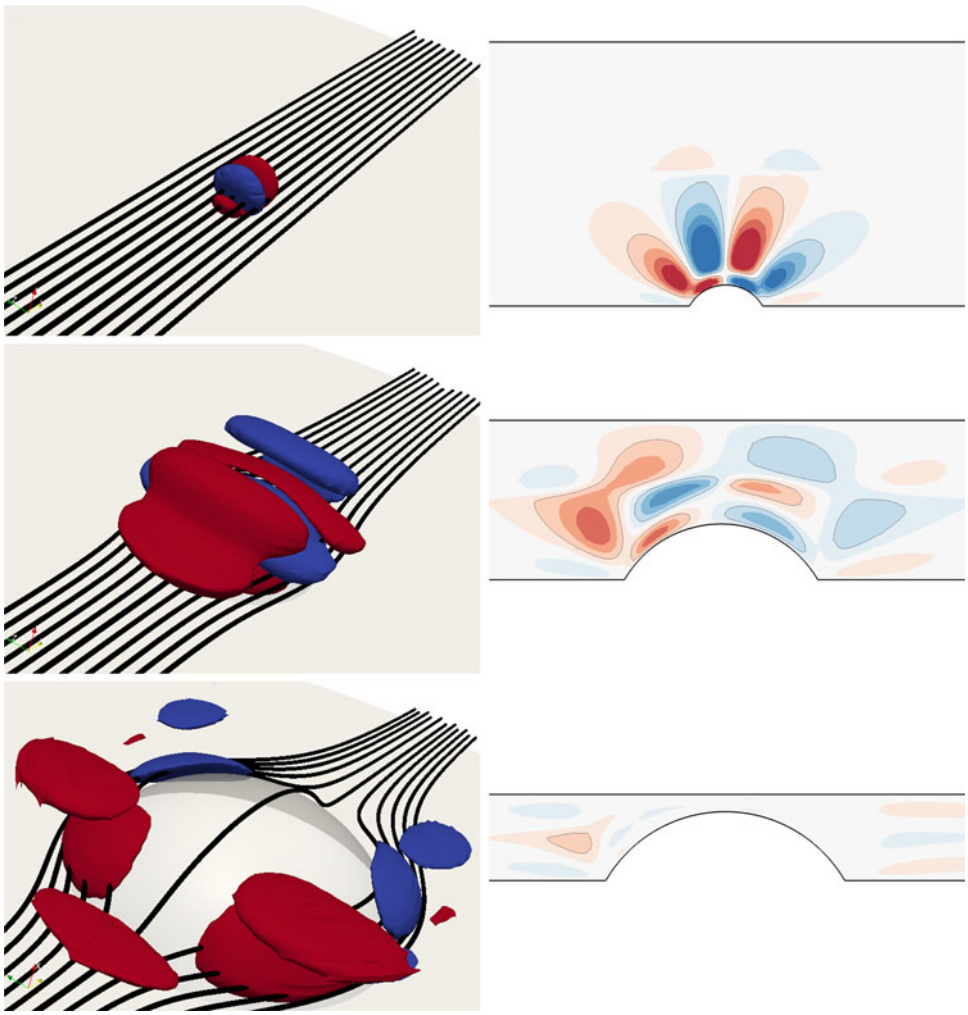

Fig. 7 Plots of ψ around thrombi at $\gamma_{Pw} = 3{,}000$. In each case an isometric view of three-dimensional isosurfaces (*left*) and a contour sliced along the flow centreline (*right*) are shown. From *top* to *bottom*, $h_t = 0.08$, 0.35 and 0.8 are shown, respectively. Isosurface frames: the flow is from the bottom left to the top right corner of the frame. The *black tubes* represent stream lines seeded upstream at $h_i = 0.2$. In each of the frames the view point is constant. The *translucent grey surface* represents the lower wall of the channel including the thrombus. The *red* and *blue* isosurfaces represent Dχ/Dt* = $\pm$ 0.25, respectively. Contour frames: the flow in each frame is from left to right across the page. Unlike the isosurface frames the view is zoomed for clarity in each case. Positive and negative contours are represented by *red* and *blue* colours, respectively. Contour levels are separated by $\Delta\psi = 0.05$ (colour figure online)

In Fig. 6 three peaks of $\max\|\psi\|$ are observed with respect to h_i. The three peaks are marked with fit lines and are labelled (in terms of increasing h_i) as P_1, P_2 and P_3, respectively. The overall peak $\max\|\psi\|$ is observed for small thrombus sizes with introduction sites near the lower wall of the channel, on P_1. Figure 2 would imply that peak $\max\|\psi\|$ would be observed for the smallest case; however, it is observed at $h_t = 0.05$. This is attributed to the relatively coarse resolution of the particles with respect to the thrombus when h_t approaches zero.

The P_1 peak is the closest peak to the lower channel surface. This behaviour is observed for all the h_t considered. As h_t increases a gradual increase in h_i of P_1 is observed. The close localisation to the surface suggests that it is likely that P_1 would stimulate platelet adhesion. It is noted that, unlike $\chi, \max\|\psi\|$ for each peak decreases through the full range of h_t. That the height of peak $\max\|\psi\|$ is non-zero is in contrast to the gradients with respect to the displacement along a platelet path $\partial\chi/\partial\mathbf{x}$. For these gradients, due to the extrema presented at the surface, the spatial gradients peak at the thrombus surface, with platelets flowing along the centre axis of the flow experience no shearing stresses (data not shown).

Also, in contrast to the spatial gradients is the P_2 peak. This peak occurs below the centreline ($h = 0.5$) of the channel. This peak results from a balance between increasing velocity and decreasing χ as h_i increases. An increase in h_i is also observed for P_2. This occurs in a linear fashion with respect to h_t until a transition occurs at $h_t \approx 0.2$. This behaviour is similar to the previously observed dynamics of $\hat{\chi}$. However, above this point a third peak (P_3) is observed where $h_i > 0.5$ for P_3. This peak approaches the upper channel wall at the limits of large h_t.

The behaviour of these peaks is interesting from a biological standpoint. Given the presumption of $|\psi|$-mediated platelet aggregation it suggests multiple regions of platelet aggregation may occur within in vitro experiments. Specifically while one peak of maximum shear gradient ($\max\|\psi\|$) remains localised near the surface, two other peaks occur well away from the channel wall, and therefore the thrombus. Additionally, the platelet aggregation may be stimulated close to the far wall, especially for very large thrombi. Figure 1c from [16] is suggestive that this may occur (aggregation is noted near the far wall). Figure 7 attempts to understand the peaks with respect to the local thrombus geometry, rather than the upstream introduction location of the platelets relative to the thrombus. Unlike in vivo flow the in silico flows are steady state both with respect to both geometry and fluid velocity. Therefore, the overall structure of the shear rate maximum may be mapped to the geometry as it is invariant with respect to time. Figure 7 shows this map.

First, we will focus on the isometric view. The progression of frames (with respect to increasing size) shows the splitting of the peak of χ into two peaks, such as in Fig. 4. For $h_t = 0.08$ the isosurfaces appear on the centreline of the flow. Careful examination of the ψ field has shown that the peak of ψ occurs at the centreline (data not shown).

Examining the contour slice (right hand frame) the multiple maxima and minima are clearly seen. The leading edge ψ maximum comprises two peaks: one protruding upwards and forwards into the flow, the other localised near the thrombus surface. A trailing tertiary peak is also observed protruding into the flow past the apex of the thrombus. However, this peak is detached from the surface, below it a negative peak is observed to occur. Therefore, three peaks of ψ are observed in the region of Fig. 6 where two peaks of ψ are observed. This is attributed to the negligible separation with respect to h_i of two of the peaks.

The flow shows two regimes close to the thrombus. One is localised on the thrombus surface where a shear increase followed by a shear decrease is observed. The other shows the variation occurring twice in succession. This suggests that any ψ-dependent behaviour will occur in multiple locations within the flow.

The second set of frames ($h_t = 0.35$) occurs just at the transition point between one and two γ_{Pw} peaks. The forward isosurfaces appear to be focused on the centreline. However, the trailing $D\chi/Dt^*$ maxima shows two distinct bulges on each side where the peaks are located. However, in this case, there is an additional set of maxima and minima occurring closer to the upper wall. It is this set of maximum and minimum that is causing the third streak in Fig. 6.

The final frames ($h_t = 0.8$) show the extreme case where χ peaks are clearly split. Consequently, at $h_t \geq 0.4$ the ψ maxima and minima have split into two symmetric lobes about the centreline. However, the forward protruding ψ maximum has stayed at the centreline. The streamtubes suggest that this peak is located where the flow first significantly diverges around the thrombus, thus as the curvature rapidly increase so does ψ.

4 Discussion

Nesbitt et al. [16] showed that artificially induced χ variations induce platelet adhesion. Additionally, Tolouei et al. [24] showed a linear correlation between steady thrombus size and γ_{Pw}. However, Fig. 2 shows that the fluid mechanical response of the system with respect to increasing γ_{Pw} is non-linear, stemming from the advection terms in the Navier–Stokes equations. Under some circumstances, for example low γ_{Pw} and h_t, the non-linear

effects will be insignificant. However, given that in vitro and in vivo thrombus geometries may be complex there is no simple way to estimate even peak γ within the system.

Platelet aggregation has previously been classified into different modes, delineated on the magnitude of γ_{Pw}: at $\gamma_{Pw} \geq 10{,}000$, pathological conditions occur where shear triggers platelet activation [7]. Conversely at low shear rates ($\gamma_{Pw} \leq 1{,}000$), platelet bonding is dominated by diffusion driven platelet activation and fibrinogen bonding [9]. However, over the middle range of shear rates, which were examined in this paper, the platelet aggregation is initially driven by mechanotransduction mediated by vWF [15, 16]. Here, we have shown a remarkable phenomena. For a simple thrombus analogue, under the non-pathological flow regime investigated, the localized shear rate more then doubles. This has the potential to trigger pathological behaviour. An example: at $\gamma_{Pw} = 7{,}500$ our experiments showed a local peak shear rate of $\gamma = 15{,}000$ well into the pathological regime.

The changes in peak shear rate observed are dependent on γ_{Pw}. However, more importantly, the behaviour is dependent on the Reynolds number of the system (Eq. 1). While there is a linear relationship between γ_{Pw} and Re, thus the results here are only applicable to the same sized geometry. However, generically there is a non-linear relationship between γ_{Pw} and the peak shear rate requiring careful investigation for each in vitro experiment considered.

Figures 3 and 4 showed that the location, and geometric structure, of the shear rate extrema surrounding the thrombus was dependent on both the γ_{Pw} and the h_t. Given γ-dependent platelet adhesion, the location of extrema within the flow will affect the locations of platelet adhesion. The behaviour observed suggests that this transition may help limit the size to which thrombi will grow within the channel (the asymptotic behaviour of the height of maximum γ for $h_t \geq 0.5$). However, this behaviour is anticipated to be strongly dependent on the geometry of the thrombus.

Given shear-stimulated thrombus growth, other growth-limiting behaviour is observed within the system. For $h_t \leq 0.5$, decreasing shear rate was observed with increasing thrombus size. Thus, if exceeding a critical shear rate is required, self–similar thrombus growth will eventually drop the shear rate such that a stable thrombus size is formed.

Conversely, as h_t increases past 0.5 there is a positive feedback mechanism for $\hat{\chi}$; as the thrombus 'grows', so too does $\hat{\chi}$. This is consistent with dangerous occlusive run-away thrombosis. If χ remains high enough, the blockage of the channel by the increasing size of the thrombus will increase χ. Thus, positive biophysical feedback loop is formed promoting thrombus growth. This behaviour, based solely on the maximum γ experienced does agree with previous experiments such as [16, 24]. This suggests that mechanotransduction may be an underlying mechanism of occlusive thrombosis.

We theorise that temporal gradients, ψ, are the most important shear rate gradients, due to the small size of platelets with respect to the flow features. These are the gradients to which platelets are exposed, given their infinitesimal size relative to the system. The behaviour of $\max||\psi||$ within the system shows the same negative feedback with respect to increasing thrombus size.

However, unlike the peak shear rate, the dominant behaviour is of decreasing ψ with increasing h_t. The location of the maxima and minima of ψ is suggestive to its relevance for platelet adhesion. The near wall maximum (P_1), seen in both Figs. 6 and 7, is located in an ideal position to promote adhesion; close to the wall of the channel where platelets flow within in vitro and in vivo flows and the platelets pass close to the rear adhesion zone of the thrombus identified in [16] such that bonding may be established. This suggests that ψ may be the appropriate parameter to measure the biomechanical effects of blood on thrombus growth.

Additionally, it is noted that multiple maxima and minima of ψ extend into the flow geometry. This suggests that platelet–platelet adhesion may occur within the flow rather than just at the flow–thrombus boundary. However, this would be difficult to ascertain experimentally using current in vitro and in vivo techniques.

Complex non-linear behaviour observed of biologically relevant flow parameters showed previously unrevealed complexity to in vitro thrombotic conditions. Critically localised flow behaviour highlights the importance of quantifying in vitro flows around each thrombus.

Acknowledgments The authors thank the Monash eResearch Centre (MeRC) for access to their central compute facility. KR and CJB thank VLSCI for the time granted on their peak compute facility under RAS Grant VR0023. G.J.S. thanks VLSCI for access to their peak compute facility under RAS Grant VR0025, and NCI for access to their National Facility through a Merit Allocation Scheme Grant. NCI is supported by the Australian Commonwealth Government. G.J.S. received financial support from a Monash University Faculty of Engineering Small Grant.

References

1. Akima H (1970) A new method of interpolation and smooth curve fitting based on local procedures. J ACM 17(4):589–602
2. Andrews RK, Berndt MC (2004) Platelet physiology and thrombosis. Thromb Res 114(5-6):447–453
3. Blackburn HM, Sherwin SJ (2004) Formulation of a Galerkin spectral element-Fourier method for three-dimensional incompressible flows in cylindrical geometries. J Comput Phys 197(2):759–778

4. Born GVR (1977) Fluid-mechanical and biochemical interactions in haemostasis. Br Med Bull 33(3):193–198
5. Brass L (2009) In the shadow of the thrombus. Nat Med 15:607–608
6. Coppola G, Sherwin S, Peirò J (2001) Nonlinear particle tracking for high-order elements. J Comput Phys 172(1):356–386
7. Dopheide SM, Maxwell MJ, Jackson SP (2002) Shear-dependent tether formation during platelet translocation on von Willebrand factor. Blood 99(1):159–167
8. Eisenberg PR, Ghigliotti G (1999) Platelet-dependent and procoagulant mechanisms in arterial thrombosis. Int J Cardiol 68:3–10
9. Furie B, Furie BC (1988) The molecular basis of blood coagulation. Cell 53(4):505–518
10. Goncalves I, Nesbitt WS, Yuan Y, Jackson SP (2005) Importance of temporal flow gradients and integrin αIIbβ_3 mechanotransduction for shear activation of platelets. J Biol Chem 280(15):15,430–15,437
11. Karniadakis GE, Israeli M, Orszag SA (1991) High-order splitting methods for the incompressible Navier–Stokes equations. J Comput Phys 97:414–443
12. Ku DN (1997) Blood flow in arteries. Annu Rev Fluid Mech 29(1):399–434
13. Kulkarni S, Dopheide SM, Yap CL, Ravanat C, Freund M, Mangin P, Heel K, Street A, Harper I, Lanza F et al (2000) A revised model of platelet aggregation. J Clin Invest 105(6): 783–791
14. Kulkarni S, Nesbitt WS, Dopheide SM, Hughan SC, Harper IS, Jackson SP (2004) Techniques to examine platelet adhesive interactions under flow. Methods Mol Biol 272:165–186
15. Maxwell MJ, Westein E, Nesbitt WS, Giuliano S, Dopheide SM, Jackson SP (2007) Identification of a 2-stage platelet aggregation process mediating shear-dependent thrombus formation. Blood 109(2):566–576
16. Nesbitt WS, Westein E, Tovar–Lopez FJ, Tolouei E, Mitchell A, Fu J, Carberry J, Fouras A, Jackson SP (2009) A shear gradient-dependent platelet aggregation mechanism drives thrombus formation. Nat Med 15(6):665–673
17. Papanastasiou T, Georgiou G, Alexandrou A: Viscous fluid flow. CRC Press, Boca Raton (2000)
18. Rodkiewicz CM, Sinha P, Kennedy JS (1990) On the application of a constitutive equation for whole human blood. J Biomech Eng T ASME 112:198–206
19. Savage B, Almus-Jacobs F, Ruggeri ZM (1998) Specific synergy of multiple substrate–receptor interactions in platelet thrombus formation under flow. Cell 94(5):657–666
20. Savage B, Saldivar E, Ruggeri ZM (1996) Initiation of platelet adhesion by arrest onto fibrinogen or translocation on von Willebrand factor. Cell 84:289–297
21. Sheard GJ (2009) Flow dynamics and wall shear-stress variation in a fusiform aneurysm. J Eng Math 64(4):379–390. doi: 10.1007/s10665-008-9261-z
22. Sheard GJ, Fitzgerald J, Ryan K (2009) Cylinders with square cross-section: wake instabilities with incidence angle variation. J Fluid Mech 630:43–69
23. Sheard GJ, Leweke T, Thompson MC, Hourigan K (2007) Flow around an impulsively arrested circular cylinder. Phys Fluids 19(8):083601
24. Tolouei E, Butler CJ, Fouras A, Ryan K, Sheard GJ, Carberry J (2011) Effect of hemodynamic forces on platelet aggregation geometry. Ann Biomed Eng 39(5):1403–1413
25. Wootton DM, Ku DN (1999) Fluid mechanics of vascular systems, diseases, and thrombosis. Annu Rev Biomed Eng 1(1):299–329